Journal of Materials Chemistry B

ROYAL SOCIETY OF CHEMISTRY

PAPER

View Article Online
View Journal | View Issue

Cite this: *J. Mater. Chem. B*, 2026, **14**, 5051

Glucagon-like peptide-1 mimotopes screened from an Fv-antibody library

Hyung Eun Bae,[a] Dayoung Choi,[b] Jeong Soo Sung,[a] Hyun Woong Lee,[c] Min-Jung Kang,[d] Joachim Jose,[e] Misu Lee*[b] and Jae-Chul Pyun*[a]

Received 21st September 2025,
Accepted 24th March 2026

DOI: 10.1039/d5tb02128f

rsc.li/materials-b

Glucagon-like peptide-1 receptor (GLP-1R) agonists treat type 2 diabetes and obesity by promoting insulin secretion and suppressing glucagon release. In this study, GLP-1 mimotopes with GLP-1R agonist activity were screened from the Fv-antibody library. The Fv-antibodies represented the hypervariable region of heavy-chain IgG, which included three CDRs and four FRs, and the library was produced by randomizing the CDR3 region with 11 amino acids through site-directed mutagenesis. The GLP-1 mimotopes with GLP-1R agonist activity were screened using monoclonal anti-GLP-1 antibodies and were synthesized into peptides and expressed as Fv-antibodies co-expressed with GFP. The binding affinity of GLP-1 mimotopes was analyzed using a surface plasmon resonance biosensor, and the activity of the GLP-1 mimotopes (expressed Fv-antibodies and synthesized peptides) was analyzed by measuring cyclic adenosine monophosphate (cAMP) production and hormone secretion in pancreatic α- and β-cells. The molecular docking simulations revealed that GLP-1 mimotopes interacted with GLP-1R by targeting key residues known to bind GLP-1, supporting their potential as functional receptor agonists. The effect on fatty acid accumulation was analyzed using hepatocyte cell lines (HepG2 and Huh7), and transcriptomic changes were analyzed by RNA sequencing. In addition, GLP-1R downstream signaling in β-cells was evaluated by western blot analysis of AKT and ERK1/2 phosphorylation. This approach offers a novel strategy to generate new GLP-1R agonists and expand molecular diversity for GLP-1R-targeted therapeutic design.

1. Introduction

Glucagon-like peptide-1 (GLP-1) is an incretin hormone secreted by enteroendocrine L-cells in response to nutrient intake.[1,2] GLP-1 exerts multiple physiological effects, including glucose-dependent insulin secretion, glucagon release suppression, delayed gastric emptying, and promotion of satiety *via* central nervous system signaling.[3–5] The GLP-1 receptor (GLP-1R) is a class B G protein-coupled receptor widely expressed in pancreatic β-cells and various peripheral tissues and plays a key role in glucose homeostasis and energy metabolism.[6,7] Several GLP-1R agonists (GLP-1RAs) such as exenatide, liraglutide, and semaglutide have been developed and approved for treating type-2 diabetes mellitus and obesity to overcome the rapid inactivation of native GLP-1 by dipeptidyl peptidase-4.[8,9] In addition to glycemic control, GLP-1RAs have shown potential therapeutic benefits in cardiovascular diseases, neurodegenerative disorders, and inflammatory conditions.[10,11]

Fragment variable (Fv)-antibodies represent variable regions of immunoglobulin G (IgG) with three complementarity-determining regions (CDRs) flanked by framework regions (FRs).[12,13] Among these, the CDR3 region of the variable heavy chain (V_H) exhibits the highest variability and plays a dominant role in determining antigen-binding specificity.[14,15] Notably, our Fv-antibodies lack the IgG constant Fc region and therefore do not engage Fc receptor or complement (C1q)-mediated effector functions.[16] An Fv-antibody library was produced by randomizing an 11-amino acid sequence of the V_H-CDR3 region through site-directed mutagenesis.[17,18]

The resulting library was genetically connected to the autotransporter domain of AIDA-1 and expressed on the outer membrane of *Escherichia coli* using autodisplay technology.[19,20] This surface display system achieved a high-density expression of Fv-antibodies ($>10^5$ molecules per *E. coli*) and provided high diversity ($>10^6$ clones per library), enabling efficient screening without the need for multiple rounds of biopanning.[21–23] This approach facilitated the identification of mimotopes, which are

[a] *Department of Materials Science and Engineering, Yonsei University, 50 Yonsei-Ro, Seodaemun-Gu, Seoul, 03722, Korea. E-mail: jcpyun@yonsei.ac.kr; Fax: +82 2 312 5375; Tel: +82 2 2293 5509*
[b] *Division of Life Sciences, College of Life Science and Bioengineering, Incheon National University, Incheon, 22012, Korea. E-mail: misulee@inu.ac.kr*
[c] *Division of Gastroenterology, Gangnam Severance Hospital, Seoul, 06273, Korea*
[d] *Korea Institute of Science and Technology, Seoul, 02456, Korea*
[e] *Institute of Pharmaceutical and Medical Chemistry, University of Munster, Münster, 48149, Germany*

short peptide sequences that mimic the structure of natural epitopes and bind specifically to target antibodies or receptors, directly from the displayed library.[24,25] This platform was successfully used to identify the amino acid sequences with binding affinity to various targets. For example, the Fv-antibody library was used to screen inhibitors specific to deoxyribonuclease I (DNase I) and β-lactamase, which demonstrated the applicability of this system to select mimotopes or inhibitory fragments for diverse protein targets.[26,27]

In this study, GLP-1 mimotopes were screened from an Fv-antibody library using an anti-GLP-1 antibody. Screened amino acid sequences (CDR3 sequences, 11 residues) were synthesized into peptides and expressed as Fv-antibodies co-expressed with GFP. The binding affinity (K_D) values of GLP-1 mimotopes were analyzed using an SPR biosensor. The activity of the GLP-1 mimotopes (expressed Fv-antibodies and synthesized peptides) was analyzed by measuring cyclic adenosine monophosphate (cAMP) production and insulin secretion. Glucagon suppression was evaluated by measuring glucagon secretion in pancreatic α-cell models. In addition, downstream GLP-1R signaling was examined *via* western blot analysis. The effect on fatty acid accumulation was analyzed using hepatocyte cell lines such as HepG2 and Huh7. The effect of GLP-1 mimotopes on gene expression was analyzed *via* RNA sequencing (RNA-seq). Accordingly, GLP-1 mimotopes were screened using an Fv-antibody library and their biological activities were characterized, providing a potential alternative strategy for the development of GLP-1RAs.

2. Materials and methods

2.1. Materials

Anti-GLP-1 antibody [4F3] (ab23472) was purchased from Abcam (Cambridge, UK). The materials necessary to produce the Fv-antibody library were described previously.[26,27] Isopropyl β-D-1-thiogalactopyranoside (IPTG) and kanamycin were purchased from Kisan Bio (Seoul, Korea). Dynabeads™ protein G was purchased from Thermo Fisher Scientific Inc. (Waltham, MA, USA). Beta-TC-6 cells (ATCC CRL-3605) and alpha-TC-1 clone 6 cells (ATCC CRL-2934) were purchased from the American Type Culture Collection (Manassas, VA, USA). HepG2 (KCLB No. 88065) and Huh7 (KCLB No. 60104) cells were obtained from the Korean Cell Line Bank (Seoul, Korea) and cultured according to the manufacturer's instructions. Furthermore, cAMP levels were measured using the cAMP-Glo assay (Promega, Madison, WI, USA). Insulin levels were measured using a rat/mouse insulin ELISA kit (EZRMI-13K; Merck Millipore, Billerica, MA, USA), and glucagon levels were measured using a Glucagon ELISA kit (EIA-GLU-1; RayBiotech, Peachtree Corners, GA, USA). 3-Isobutyl-1-methylxanthine (IBMX I5879) was purchased from Sigma-Aldrich (St. Louis, MO, USA). The Krebs-Ringer-Bicarbonate buffer with 16.7 mM glucose (BK010) and Krebs-Ringer-Bicarbonate buffer with 2.8 mM glucose (BK009) were purchased from Biosolution (Seoul, Korea). Exendin-4 (HY-13443) was purchased from MedChemExpress (Monmouth Junction, NJ, USA). Synthetic human GLP-1 (7–36), semaglutide, and tirzepatide were purchased from Dandicure (Cheongju, Korea). The identity and purity of the synthetic peptides were verified by analytical RP-HPLC and MS, and the corresponding data are provided in Fig. S1.

2.2. Mimotope screening from the Fv-library

The Fv-antibody library was constructed using site-directed mutagenesis.[26,27] The CDR3 sequences, including 11-mer randomized amino acids, were synthesized using the NNK codon strategy and inserted into an expression vector harboring the AIDA-1 autotransporter system. The resulting plasmids were transformed into *E. coli* BL21(DE3), which enables the surface display of Fv-antibodies on the outer membrane. Furthermore, the transformed cells were incubated in LB broth (10 mL) with 50 mg L^{-1} kanamycin (37 °C, 200 rpm, 16 h), which is followed by incubation in the LB broth (10 mL) containing kanamycin (50 mg L^{-1}), β-mercaptoethanol (10 mM), and EDTA (10 μM) at 37 °C for 2.5 h. Subsequently, autodisplay expression was induced with isopropyl β-D-1-thiogalactopyranoside (IPTG, 1 mM).

A monoclonal anti-GLP-1 antibody was immobilized on Dynabeads™ Protein G (Thermo Fisher Scientific) according to the manufacturer's instructions for screening GLP-1 mimotopes. The autodisplayed Fv-antibody library (OD_{600nm} = 1.0) was incubated with immobilized monoclonal anti-GLP-1 antibodies (25 °C, 1 h). The *E. coli* clones exhibiting strong binding affinity to the antibody were isolated by magnetic bead capture, which includes washing with 0.01% (v/v) PBST and PBS. After washing, screened *E. coli* clones were plated onto an agar plate (37 °C, overnight). For selecting the final clones, candidate colonies were randomly picked from the agar plate and incubated with a monoclonal anti-GLP-1 antibody (5 μg mL^{-1}) followed by FITC-labeled secondary antibody (5 μg mL^{-1}). Clones exhibiting strong fluorescence signals were identified by flow cytometry (FACSCalibur; Becton Dickinson, USA) and subjected to DNA sequencing. The selected clones were subsequently expressed as soluble recombinant proteins in *E. coli* using plasmids pHE006 and pHE007 and synthesized into peptides by Peptron (Daejeon, Republic of Korea). The Fv sequences of the selected clones (including Fv-5 and Fv-8) are summarized in Table S1.

2.3. cAMP measurement

Intracellular cAMP levels were measured using the cAMP-Glo™ assay kit (Promega, Madison, WI, USA) based on the manufacturer's protocol.[28] Beta-TC-6 cells were cultured in Dulbecco's modified Eagle's medium (DMEM; BioWest, L0103) supplemented with 15% fetal bovine serum (FBS; BioWest, S1480) and 2% penicillin–streptomycin (Thermo Fisher Scientific, 15140122) at 37 °C and 5% CO_2.[29–31] Beta-TC-6 cells were seeded into 96-well plates at a density of 2.5×10^4 cells per well and cultured for 2–3 days. Prior to treatment, the cells were pre-incubated with either 2.8 or 16.7 mM glucose-containing Krebs-Ringer buffer in the presence of 0.5 mM IBMX for 1.5 h to inhibit phosphodiesterase activity.[32] Then, the buffer was

replaced with the same glucose-containing buffer supplemented with Fv-5, Fv-8, Exendin-4, semaglutide, or tirzepatide at concentrations ranging from 0.32 to 1000 nM, or with Peptide-5 or Peptide-8 at concentrations ranging from 1.6 to 5000 nM. After 1 h of incubation at 37 °C, the cells were lysed, and luminescence was measured using a microplate reader. Intracellular cAMP concentrations were quantified by comparing the measured luminescence to a standard curve generated from cAMP standards based on the manufacturer's instructions.

2.4. Insulin measurement

Beta-TC-6 cells were seeded into 96-well plates at a density of 2.5×10^4 cells per well and cultured for 2–3 days. Prior to stimulation, the cells were pre-incubated under the same conditions used for cAMP measurement: Krebs-Ringer buffer (KRB) containing either 2.8 or 16.7 mM glucose and 0.5 mM IBMX for 1.5 h at 37 °C.[33,34] Then, the buffer was replaced with glucose-containing KRB supplemented with Fv-5, Fv-8, Exendin-4, semaglutide, or tirzepatide at concentrations ranging from 0.32 to 1000 nM, or with Peptide-5 or Peptide-8 at concentrations ranging from 1.6 to 5000 nM, followed by a 1 h incubation. After stimulation, the supernatants were collected, and insulin secretion into the medium was quantified using a Rat/Mouse Insulin ELISA kit based on the manufacturer's instructions.[35,36]

2.5. Glucagon measurement

Alpha-TC-1 clone 6 cells were seeded at 5.0×10^4 cells per well and cultured for 2–3 days. Cells were washed with DPBS and pre-incubated for 1.5 h at 37 °C in Krebs-Ringer buffer (KRB) containing either 2.8 mM or 16.7 mM glucose. The buffer was replaced with the same glucose-containing buffer supplemented with Fv-5, Fv-8, Exendin-4, semaglutide, or tirzepatide at concentrations ranging from 0.32 to 1000 nM. Control wells received glucose-matched KRB without ligands. After 1 h incubation at 37 °C, the supernatants were collected and glucagon levels were quantified using a glucagon ELISA kit according to the manufacturer's instructions.

2.6. Hormone secretion assays in α/β Co-spheroids

Alpha-TC-1 clone 6 cells and beta-TC-6 cells were co-cultured to generate α/β co-spheroids. To generate stable mCherry-expressing beta-TC-6 cells, lentiviral particles were produced by co-transfecting Lenti-X™ HEK293T cells (Clontech, Palo Alto, CA, USA) with the packaging plasmid psPAX2 (Addgene, Watertown, MA, USA), the envelope plasmid pCMV-VSV-G (Addgene, Watertown, MA, USA), and the transfer vector pLVX-mCherry (Addgene). Supernatants were harvested and concentrated using the Lenti-X™ Concentrator (Takara Bio Inc., Shiga, Japan) according to the manufacturer's protocol. Beta-TC-6 cells (6×10^5 cells per well) were seeded in six-well plates and infected 24 h later with the prepared viral particles diluted in medium containing 2% heat-inactivated fetal bovine serum and 1% penicillin–streptomycin. The cells were mixed at a 1 : 3 ratio (α-TC1-6 : mCherry-β-TC-6), corresponding to 7.5×10^3 α-cells and 22.5×10^3 β-cells per spheroid (3.0×10^4 total cells per spheroid), and seeded into ultra-low attachment 96-well plates to allow the formation of a single spheroid per well. For each condition, 10 co-spheroids were pooled and used as one experimental unit. Prior to stimulation, co-spheroids were washed with DPBS and pre-incubated for 1.5 h at 37 °C in Krebs-Ringer buffer (KRB) containing either 2.8 mM or 16.7 mM glucose supplemented with 0.5 mM IBMX. The buffer was then replaced with new glucose-matched KRB containing Fv-5, Fv-8, Exendin-4, semaglutide, or tirzepatide (1 μM each), while control spheroids received the corresponding buffer without agonists. After 1 h of incubation at 37 °C, supernatants were collected for insulin and glucagon measurement by ELISA according to the manufacturer's instructions. Co-spheroids were subsequently lysed, and intracellular cAMP levels were measured using the cAMP-Glo™ assay as described above (Section 2.3).

2.7. Western blot analysis of intracellular signaling (AKT and ERK1/2)

Beta-TC-6 cells were seeded in 6-well plates at a density of 2.5×10^5 cells per well and cultured for 2–3 days. Prior to stimulation, the cells were washed with DPBS and pre-incubated for 1.5 h at 37 °C in Krebs-Ringer buffer (KRB) containing either 2.8 mM or 16.7 mM glucose. The buffer was then replaced with fresh KRB adjusted to either low glucose (2.8 mM) or high glucose (16.7 mM) and supplemented with Fv-5, Fv-8, or Exendin-4 (1 μM). After incubating for 1 h at 37 °C, the cells were lysed using an SDS-based lysis buffer (1% SDS, 60 mM Tris-HCl) supplemented with a protease inhibitor cocktail (Roche, Basel, Switzerland) and a phosphatase inhibitor (GenDEPOT, Barker, TX, USA). Total protein concentrations were measured using a BCA assay. Equal amounts of protein were resolved by SDS–PAGE and electrotransferred onto PVDF membranes. After blocking with 5% skim milk, the membranes were incubated with primary antibodies at 4 °C overnight, followed by incubation with HRP-conjugated secondary antibodies. The primary antibodies used were phospho-AKT (Ser473, Cell Signaling Technology; 1 : 2000), pan-AKT (Cell Signaling Technology; 1 : 1000), phospho-ERK1/2 (Thr202/Tyr204, Cell Signaling Technology; 1 : 2000), ERK1/2 (Cell Signaling Technology; 1 : 1000), and β-actin-HRP (Santa Cruz Biotechnology; 1 : 5000). Chemiluminescent signals were visualized using a ChemiDoc XRS system (Bio-Rad, Hercules, CA, USA), and band intensities were quantified using Image Lab (BiRad) and ImageJ (NIH, Bethesda, MD, USA). Western blot analysis was carried out following standard procedures as previously described.[37]

2.8. Estimation of fatty acid accumulation

RNA sequencing was performed to assess the effect of the GLP-1 mimotope on fatty acid accumulation. HepG2 cells were seeded in 48-well plates at a density of 4×10^4 cells per mL. After 24 h, the cells were treated with Fv-5, Fv-8, or Exendin-4 in the presence of oleic acid. Following 24 h of treatment, the total RNA was extracted from the cells using the RNeasy Mini Kit (QIAGEN, Hilden, Germany). Furthermore, RNA sequencing

was performed by EBIOGEN Inc. (Seoul, Korea), and data analysis was conducted using the Database for Annotation, Visualization, and Integrated Discovery (DAVID) annotation tool.[38,39]

Oil Red O staining was performed to measure the lipid droplet content in HepG2 and Huh7 cells. Cells were seeded in 48-well plates at a density of 4×10^4 cells per mL for HepG2 and 1.5×10^4 cells per mL for Huh7. After 24 h, the cells were treated with Fv-5, Fv-8, or Exendin-4 in combination with oleic acid for an additional 24 h. The cells were washed twice with phosphate-buffered saline (PBS) and fixed with 4% paraformaldehyde for 30 min at 25 °C. After fixation, the cells were rinsed with distilled water and treated with 60% isopropanol for 5 min. The Oil Red O working solution was prepared by diluting a 0.5% (w/v) Oil Red O stock solution in isopropanol with distilled water at a ratio of 3 : 2, followed by filtration through a 0.22 μm membrane filter. Then, the cells were incubated with the oil red working solution for 30 min at room temperature. After staining, the excess dye was removed by washing with distilled water, and the cells were air-dried. Stained lipid droplets were visualized and imaged under a light microscope. For quantification, the cells were lysed with 100% isopropanol, and the absorbance was measured at 515 nm using a microplate reader.

3. Results and discussion

3.1. Screening the GLP-1 mimotope from the Fv-antibody library

Fv-antibodies represent the hyper-variable region of heavy-chain IgG, which includes three CDRs and four FRs.[40,41] The Fv-antibody library was produced by randomizing the CDR3 region with 11 amino acids through site-directed mutagenesis.[17,42] Subsequently, the Fv-antibody library was expressed on the outer membrane of *E. coli* using autodisplay technology, as shown in Fig. 1(a).[21,43] This study aimed to screen a GLP-1 mimotope from the Fv-antibody library, which had a similar chemical environment to GLP-1. A monoclonal anti-GLP-1 antibody was used as a probe in the Fv-antibody library to screen for GLP-1 mimotopes. The monoclonal antibody was immobilized on the magnetic beads *via* covalent bonding, and the magnetic beads were used to treat the Fv-antibody library, as shown in Fig. 1(b). After separating the magnetic beads, the complex of magnetic beads and *E. coli* was cultured on an agar plate. Several resulting clones were subsequently assayed using flow cytometry, as shown in Fig. 1(c).

Among the assayed clones, two clones were identified as target clones based on their distinct CDR3 sequences, which differed from the template sequence (before site-directed mutagenesis). The two clones exhibited a concentration-dependent increase in fluorescent signal upon anti-GLP-1 antibody treatment. The binding affinities (K_D) of clone-5 and clone-8, were determined to be 50.0 nM and 55.1 nM, respectively (Fig. S2).

Two screened Fv-antibodies were expressed as soluble proteins co-expressed with GFP, and their expression was

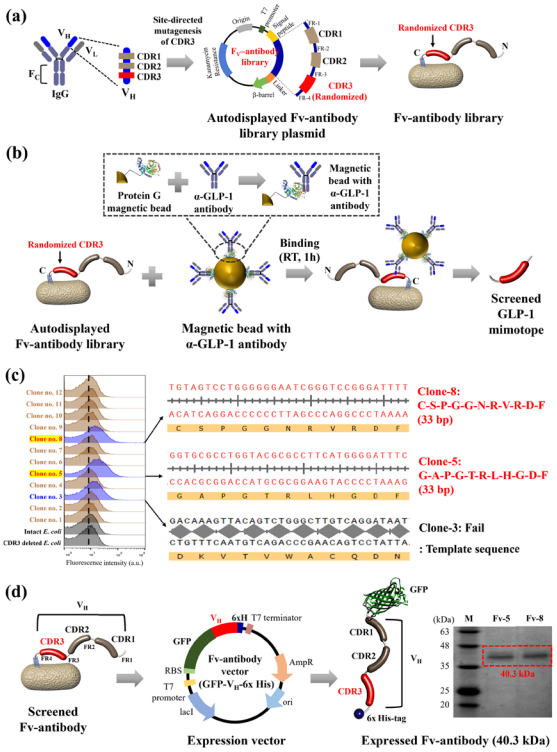

Fig. 1 Construction and screening of the Fv-antibody library targeting monoclonal anti-GLP-1 antibodies. (a) Construction of an Fv-antibody library by CDR3 randomization and outer membrane expression *via* the AIDA-1 autotransporter. (b) Screening of GLP-1 mimotopes clones using monoclonal anti-GLP-1 antibody-conjugated magnetic beads. (c) Sequencing results of the CDR3 regions from GLP-1 mimotope clones and flow cytometry analysis of the binding affinity of clone-5 and clone-8. (d) Expression of screened Fv-antibodies as a soluble protein, confirmed by SDS-PAGE showing a band at an expected molecular weight of approximately 40.3 kDa.

confirmed using SDS-PAGE with a molecular weight of 40.3 kDa, as shown in Fig. 1(d).[44]

The K_D of the expressed Fv antibodies to the immobilized monoclonal anti-GLP-1 antibody was estimated using an SPR biosensor.[45,46] As shown in Fig. S3(a), the K_D value was determined to be 71.3 and 62.8 nM for Fv-5 and Fv-8, respectively, which was similar to that for the conventional GLP-1RA called Exendin-4 (Ex-4, 66.1 nM). Under the same SPR conditions, synthetic human GLP-1 (7−36) showed an estimated K_D of 23.2 nM, whereas semaglutide and tirzepatide showed estimated K_D values of 38.3 nM and 58.0 nM, respectively (Fig. S3(c)). These results indicated that the two Fv-antibodies bound to the anti-GLP-1 antibody within a range comparable to representative GLP-1 agonist benchmarks measured under the same SPR conditions (Exendin-4, GLP-1, semaglutide, tirzepatide). The K_D values of the synthesized peptides with the same CDR3 amino acid sequence were estimated for the immobilized monoclonal anti-GLP-1 antibody using the SPR biosensor. Fig. S3(b) shows that the K_D value was 372.7 and 315.6 nM for Peptide-5 and Peptide-8, respectively. These results confirmed that Fv-antibodies had a higher affinity (lower K_D) than those in the synthesized peptides with the same CDR3 amino

Table 1 Screened nucleotide and amino acid sequences with a specific binding affinity to monoclonal α-GLP-1 antibodies

Screened CDR3		Sequences	$K_{D,FACS}$ [nM] (clone)	$K_{D,\ SPR}$ [nM] (expressed Fv)	$K_{D,\ SPR}$ [nM] (synthesized peptide)
Mimotope-5 (Clone-5)	Oligonucleotide Amino acid sequences	5′-^{1}GGTGC^{6}GCCTG^{11}GTACG^{16}CGCCT^{21}TCATG^{26}GGGAT^{31}TT^{33}C-3′ ^{1}G-A-P-G-T-^{6}R-L-H-G-D-^{11}F	50.0	71.3	372.7
Mimotope-8 (Clone-8)	Oligo-nucleotide Amino acid sequences	5′-^{1}TGTAG^{6}TCCTG^{11}GGGGG^{16}AATCG^{21}GGTCC^{26}GGGAT^{31}TT^{33}T-3′ ^{1}C-S-P-G-G-^{6}N-R-V-R-D-^{11}F	55.1	62.8	315.6

acid sequences. The oligonucleotide and amino acid sequences of the screened CDR3 sequences with specific binding affinity are summarized in Table 1.

3.2. Properties of GLP-1 mimotopes

The beta-TC-6 cell (ATCC CRL-3605) was derived from a pancreatic beta-cell with GLP-1Rs on the cell surface.[47,48] Intracellular glucose was metabolized through glycolysis and oxidative phosphorylation after glucose uptake *via* glucose transporters, which led to increased adenosine triphosphate (ATP) production. The elevated ATP/adenosine diphosphate (ADP) ratio closed ATP-sensitive K^+ channels, resulting in membrane depolarization and the opening of voltage-dependent Ca^{2+}channels. The subsequent Ca^{2+} influx triggered glucose-stimulated insulin secretion.[49,50]

In parallel, GLP-1 or its agonists bound to the GLP-1R and activated adenylate cyclase (AC), converting ATP into cAMP. An increase in cAMP levels further enhanced insulin secretion by activating PKA and Epac2, both of which increased Ca^{2+} sensitivity and promoted additional Ca^{2+} influx.[51,52]

In addition to enhancing insulin secretion, GLP-1 signaling suppressed glucagon secretion from pancreatic α-cells, which was likely through paracrine regulation by somatostatin or direct inhibition under hyperglycemic conditions.[53,54] The direct mechanism was proposed to involve the activation of GLP-1Rs on α-cells, which inhibited voltage-gated P/Q-type Ca^{2+} channels and subsequently reduced the Ca^{2+} influx necessary for glucagon exocytosis.[5,55] In this study, the bioactivity of GLP-1 mimotopes was evaluated by measuring intracellular cAMP levels and insulin secretion in beta-TC-6 cells.[56,57]

As shown in Fig. 2(a), the binding of GLP-1 mimotopes to the GLP-1R activates AC, and the cAMP level increases with the concentration of bound GLP-1 mimotopes.[32,58] The SPR-derived K_D values in this study reflected binding to the immobilized monoclonal anti-GLP-1 antibody (Fig. S3), and provided an assay-matched antibody-binding benchmark. In this SPR format, synthetic human GLP-1 (7-36) showed K_D values of 23.2 nM, and our expressed Fv-antibodies and corresponding peptides bound within a comparable range (62.8 nM-372.7 nM), supporting GLP-1-like epitope features, aligning with the agonist-like cellular responses, as evidenced by intracellular cAMP production, insulin secretion and glucagon suppression. In addition, a GLP-1R-based secondary validation was conducted using a flow-cytometry competitive binding assay in beta-TC-6 cells. Co-incubation with GLP-1 (100 nM) reduced the binding signals by 48.8% (Fv-5) and 54.1% (Fv-8) at 1 μM, supporting ligand-competitive engagement of GLP-1R (Fig. S4).

The agonist activity of the Fv-antibodies was estimated by measuring cAMP levels in beta-TC-6 cells after treatment with Fv-antibodies. As shown in Fig. 2(b), the cAMP level increased with the Fv-antibodies treatment at a low glucose concentration (2.8 mM), and the EC_{50} (half maximal effective concentration) values were measured to be 52.4 and 65.6 nM for Fv-5 and Fv-8, respectively. For Ex-4, the EC_{50} value was estimated to be 19.6 nM. The EC_{50} values were measured to be 49.7 and 58.2 nM for Fv-5 and Fv-8, respectively, when the cAMP measurement was carried out at the high glucose concentration of 16.7 mM. Treatment with Ex-4 resulted in an EC_{50} value of 18.9 nM, which confirmed that treatment with Fv-antibodies at low and high glucose concentrations increased cAMP production, indicating the agonist activity of Fv-antibodies. In the same cAMP assay, semaglutide and tirzepatide induced cAMP production with EC_{50} values of 16.7 nM and 58.8 nM at low glucose (2.8 mM), as well as 14.8 nM and 61.4 nM at high glucose (16.7 mM), respectively (Fig. 2(b)).

Furthermore, GLP-1 mimotopes were converted into synthesized peptides with CDR3 amino acid sequences (11 residues), and the agonist activity of the GLP-1 mimotope peptides was estimated by measuring cAMP levels after treatment with beta-TC-6 cells. The EC_{50} values were measured to be 185.1 and 273.0 nM for Peptide-5 and Peptide-8, respectively, when the cAMP level was at a low glucose concentration of 2.8 mM, as shown in Fig. 2(c). The cAMP level was observed at a high glucose concentration of 16.7 mM, and the EC_{50} values were measured to be 335.9 and 331.7 nM for Peptide-5 and Peptide-8, respectively. These results confirmed that GLP-1 mimotopes in the structure of Fv-antibodies had higher agonist activity than the synthesized peptides with the same CDR3 amino acid sequences. This difference in agonist activity resulted from the difference in K_D between the Fv-antibodies and synthesized peptides. Notably, the higher agonist activity of the Fv-antibodies could also be attributed to framework-mediated CDR3 preorganization relative to the corresponding synthesized peptides.[59,60] The EC_{50} values for cAMP accumulation are summarized in Table 2.

As an agonist of the GLP-1R, the binding of GLP-1 mimotopes to the receptor activates beta-TC-6 cells, and the secretion of insulin increases based on the concentration of bound GLP-1 mimotopes (Fig. 3(a)).[52,61] The insulin level was increased by treatment with Fv-antibodies at a low glucose concentration (2.8 mM), and the EC_{50} values were measured to be 118.4 and 99.1 nM for Fv-5 and Fv-8, respectively, as indicated in Fig. 3(b).

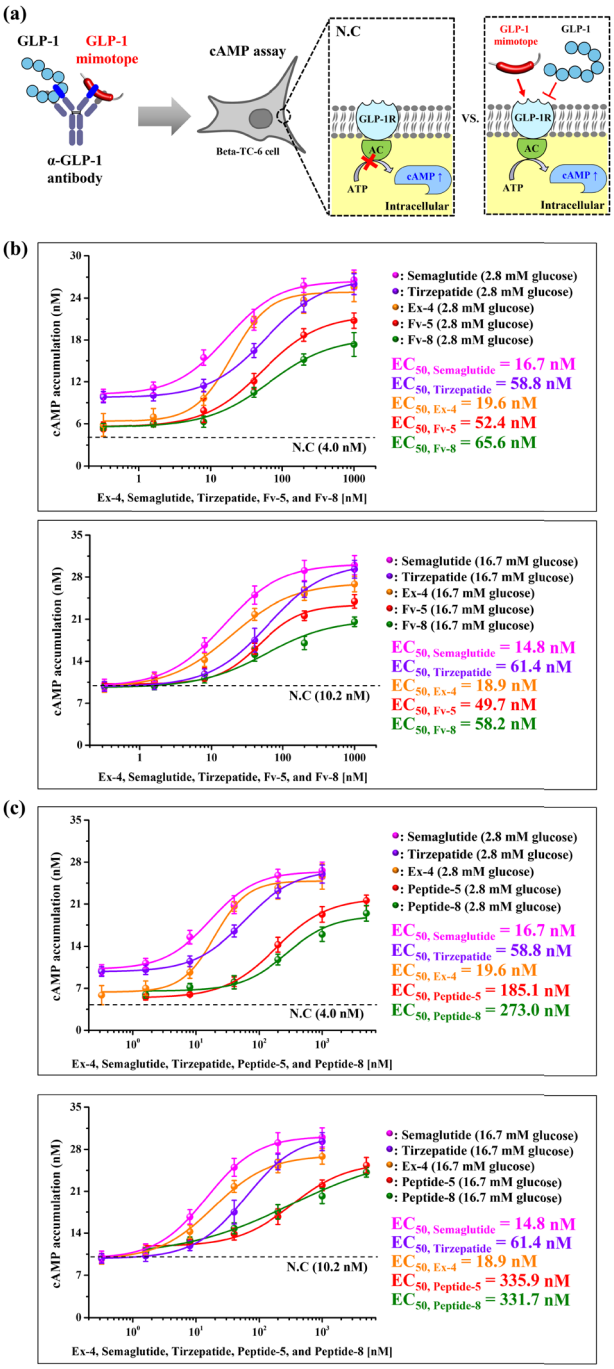

Fig. 2 EC_{50}-based evaluation of GLP-1 mimotope-induced cAMP production in beta-TC-6 cells under low and high glucose conditions. (a) Schematic of GLP-1R activation and subsequent cAMP production upon binding of GLP-1 or mimotopes in beta-TC-6 cells. (b) EC_{50} values for cAMP production induced by Fv-antibodies (Fv-5, Fv-8) and GLP-1R agonists (Ex-4, Semaglutide, Tirzepatide) under low glucose (2.8 mM) and high glucose (16.7 mM) conditions. (c) EC_{50} values for the synthesized peptides (Peptide-5, Peptide-8) under low glucose (2.8 mM) and high glucose (16.7 mM) conditions.

For Ex-4, the EC_{50} value was estimated to be 61.9 nM. When insulin levels were measured at a high glucose concentration of 16.7 mM, the EC_{50} values were 84.4 and 79.2 nM for Fv-5 and Fv-8, respectively. Treatment with Ex-4 resulted in an EC_{50} value of 55.8 nM. These results confirmed that treatment with Fv-antibodies at low and high glucose concentrations increased insulin production, indicating the agonist function of the Fv-antibodies.

Table 2 EC_{50} and maximum cAMP accumulation induced by GLP-1 mimotopes and GLP-1R agonists in beta-TC-6 cells under low and high glucose conditions

		cAMP accumulation			
		Low glucose		High glucose	
		EC_{50} [nM]	Maximum level [nM]	EC_{50} [nM]	Maximum level [nM]
Negative control		—	4.0	—	10.2
Expressed Fv-antibodies	Fv-5	52.4	20.8	49.7	24.0
	Fv-8	65.6	17.4	58.2	20.6
Synthesized peptides	Peptide-5	185.1	21.6	335.9	25.3
	Peptide-8	273.0	19.5	331.7	24.2
Exendin-4		19.6	25.6	18.9	26.8
Semaglutide		16.7	26.6	14.8	30.0
Tirzepatide		58.8	26.0	61.4	29.3

In the same insulin secretion assay, semaglutide and tirzepatide showed EC_{50} values of 56.6 nM and 81.2 nM under low glucose (2.8 mM) conditions, and 54.8 nM and 93.6 nM under high glucose (16.7 mM) conditions, respectively (Fig. 3(b)). As shown in Fig. 3(c), the agonist activity of GLP-1 mimotope peptides was estimated by measuring insulin levels in the beta-TC-6 cells after treatment. The EC_{50} values were measured to be 251.6 and 235.3 nM for Peptide-5 and Peptide-8, respectively, when the insulin level was observed at a low glucose concentration of 2.8 mM. When the insulin level was observed at a high glucose concentration of 16.7 mM, the EC_{50} values were measured to be 354.4 and 280.1 nM for Peptide-5 and Peptide-8, respectively. These results confirmed that GLP-1 mimotopes in the structure of Fv-antibodies had higher agonist activity than the peptides synthesized with the same CDR3 amino acid sequences. This difference in agonist activity could also be attributed to the difference in K_D values between the Fv-antibodies and the synthesized peptides. Notably, framework-mediated CDR3 preorganization may contribute to the higher agonist activity of the Fv-antibodies relative to the corresponding synthesized peptides.[59,60] The EC_{50} values for insulin secretion are summarized in Table 3.

The alpha-TC-1 clone 6 cell (ATCC CRL-2934) was derived from a pancreatic α-cell and secretes glucagon.[62] Glucagon secretion from α-cells is governed by glucose availability and α-cell excitability, and the secretory output is coupled to Ca^{2+} dependent exocytosis of glucagon granules.[63,64] GLP-1 and GLP-1R agonists have been reported to suppress glucagon secretion, and the proposed mechanisms include intra-islet paracrine regulation, particularly somatostatin-dependent pathways, as well as direct α-cell modulation depending on the glucose level.[65,66] Notably, GLP-1 can inhibit glucagon secretion even when detectable GLP-1R immunoreactivity is present in only a small fraction of α-cells, supporting that glucagonostatic responses may be captured in α-cell-focused assays under appropriate conditions.[5]

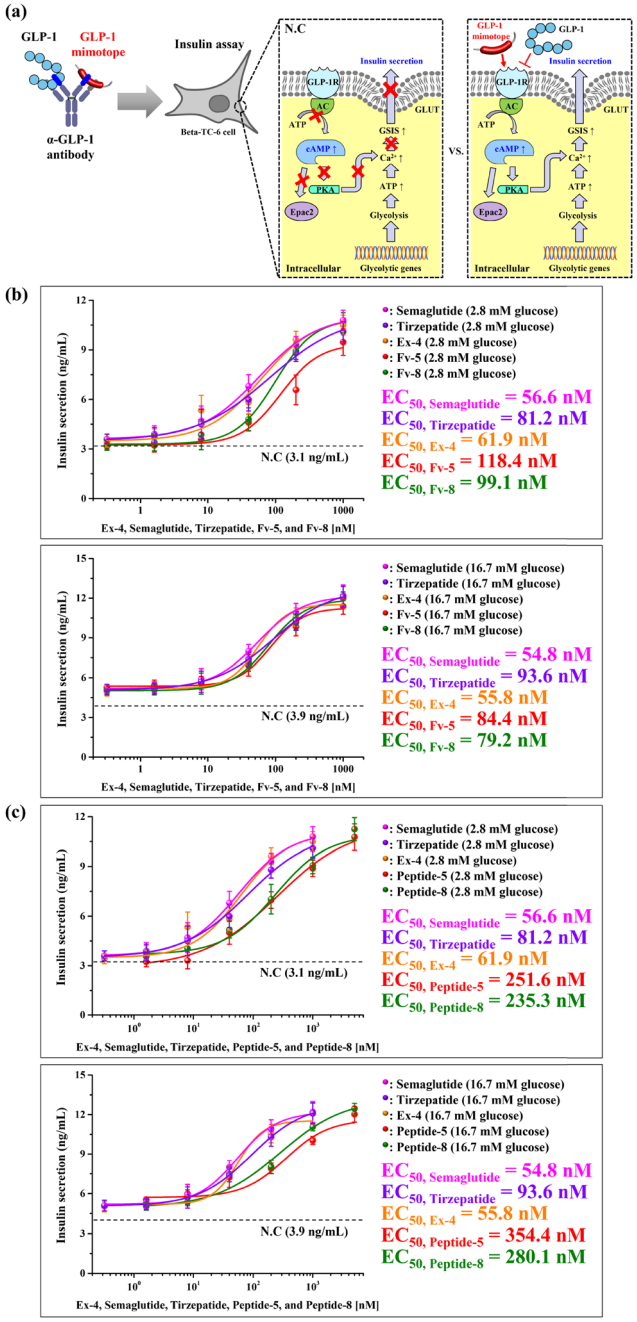

Fig. 3 EC_{50}-based evaluation of GLP-1 mimotope-induced insulin secretion in beta-TC-6 cells under low and high glucose conditions. (a) Schematic of GLP-1R activation and subsequent insulin secretion upon binding of GLP-1 or mimotopes in beta-TC-6 cells. (b) EC_{50} values for insulin secretion induced by Fv-antibodies (Fv-5, Fv-8) and GLP-1R agonists (Ex-4, Semaglutide, Tirzepatide) under low glucose (2.8 mM) and high glucose (16.7 mM) conditions. (c) EC_{50} values for the peptides (Peptide-5, Peptide-8) synthesized under low glucose (2.8 mM) and high glucose (16.7 mM) conditions.

Direct inhibitory mechanisms have been linked to reduced activity of voltage-gated Ca^{2+} channels and diminished Ca^{2+} influx required for glucagon exocytosis.[5,67] As shown in Fig. 4(a), GLP-1 mimotopes are expected to engage GLP-1R and attenuate Ca^{2+}-dependent glucagon granule exocytosis, resulting in reduced

Table 3 EC_{50} and maximum insulin secretion induced by GLP-1 mimotopes and GLP-1R agonists in beta-TC-6 cells under low and high glucose conditions

		Insulin secretion			
		Low glucose		High glucose	
		EC_{50} [nM]	Maximum level [ng mL^{-1}]	EC_{50} [nM]	Maximum level [ng mL^{-1}]
Negative control		—	3.1	—	3.9
Expressed Fv-antibodies	Fv-5	118.4	9.5	84.4	11.4
	Fv-8	99.1	10.6	79.2	12.0
Synthesized peptides	Peptide-5	251.6	10.8	354.4	12.0
	Peptide-8	235.3	11.2	280.1	12.5
Exendin-4		61.9	10.5	55.8	12.1
Semaglutide		56.6	10.8	54.8	12.2
Tirzepatide		81.2	10.1	93.6	12.1

glucagon secretion. In this study, the glucagonostatic activity of GLP-1 mimotopes was evaluated by measuring glucagon secretion in alpha-TC-1 clone 6 cells under low (2.8 mM) and high (16.7 mM) glucose conditions.

As shown in Fig. 4(b), under low glucose (2.8 mM), the glucagon level in the glucose-matched control was 45.0 pg mL^{-1}, and treatment with Fv-5, Fv-8, Ex-4, semaglutide, or tirzepatide decreased glucagon secretion in a dose-dependent manner, enabling IC_{50} estimation. The IC_{50} values were 57.0 nM for Fv-5, 70.7 nM for Fv-8, 19.2 nM for Ex-4, 35.5 nM for semaglutide, and 89.9 nM for tirzepatide. As shown in Fig. 4(c), under high glucose (16.7 mM) conditions, the glucagon level in the control was 35.1 pg mL^{-1}, and the dose-dependent effect was markedly attenuated. At 1 μM, glucagon secretion decreased by 8.3% with Fv-5, 6.6% with Fv-8, 9.4% with Ex-4, 7.7% with semaglutide, and 6.8% with tirzepatide relative to the glucose-matched control, which was not suitable for robust IC_{50} fitting within the tested range. At high glucose, glucose-driven suppression of glucagon secretion predominates, which can attenuate the additional glucagonostatic effect observed upon GLP-1/GLP-1R agonist treatment.[65]

Overall, Fv-5 and Fv-8 elicited glucagonostatic activity in alpha-TC-1 clone 6 cells, showing clear dose-dependent suppression under low glucose (2.8 mM) conditions with quantifiable IC_{50} values, comparable to GLP-1R agonist controls. Under high glucose (16.7 mM), glucagon secretion was already strongly suppressed by glucose, resulting in a limited dynamic range and only modest additional inhibition within the tested concentration range.

3.3. 3D α/β Co-spheroid validation of GLP-1 mimotopes

The bioactivity of GLP-1 mimotopes was further evaluated in a 3D pancreatic α/β co-spheroid model composed of alpha-TC-1 clone 6 and beta-TC-6 cells (α/β = 1 : 3). As shown in Fig. 5(a), the co-spheroids maintained a stable 3D architecture as confirmed by DAPI staining (blue) and mCherry-labeled β-TC-6 cells (red). In addition, FITC-labeled Fv-5 and Fv-8 (green) showed clear fluorescence signals within the co-spheroids, supporting the feasibility of assessing ligand responses in the 3D spheroid setting.

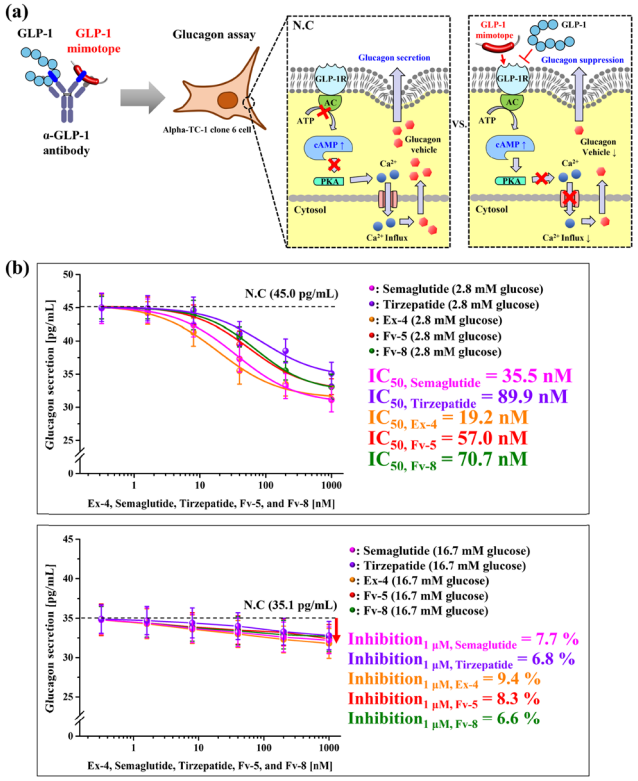

Fig. 4 IC_{50}-based evaluation of GLP-1 mimotope-induced suppression of glucagon secretion in alpha-TC-1 clone 6 cells under low and high glucose conditions. (a) Schematic of GLP-1R engagement and reduced Ca^{2+}-dependent glucagon exocytosis upon binding of GLP-1 mimotopes in alpha-TC-1 clone 6 cells. (b) Dose–response curves and IC_{50} values for glucagon suppression by Fv-antibodies (Fv-5, Fv-8) and GLP-1R agonists (Ex-4, Semaglutide, Tirzepatide) under low glucose (2.8 mM) conditions. (c) Glucagon secretion profiles under high glucose (16.7 mM) conditions, showing attenuated inhibition and no robust IC_{50} fitting within the tested concentration range.

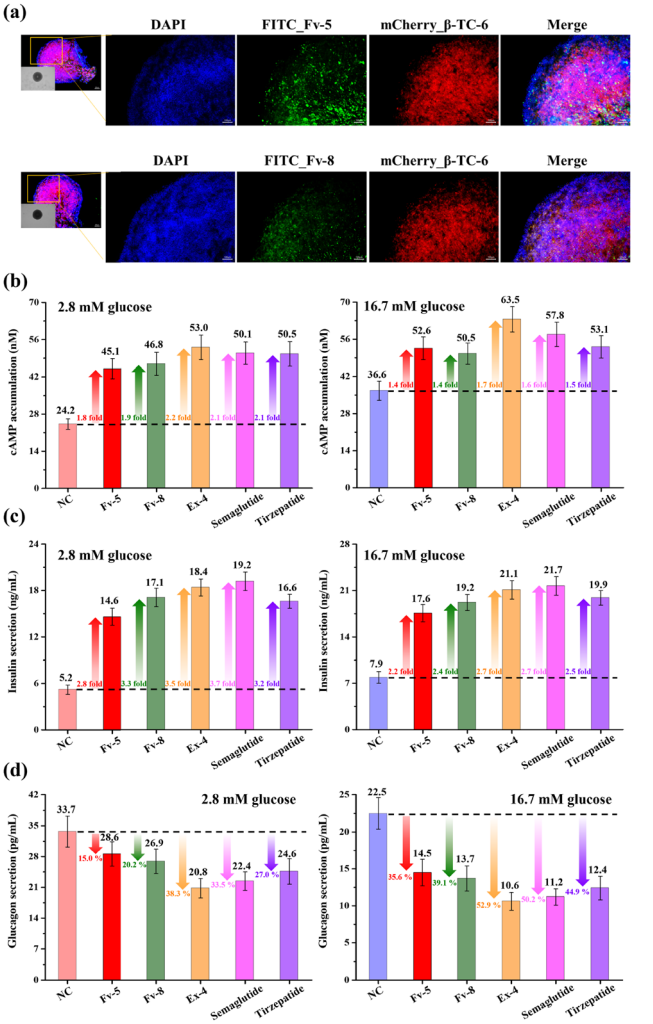

Fig. 5 3D α/β co-spheroid validation of GLP-1 mimotopes. (a) Representative fluorescence images of α/β co-spheroids (α-TC1–6 and mCherry-labeled β-TC-6, α/β = 1 : 3) incubated with FITC-labeled Fv-5 or Fv-8. Nuclei were stained with DAPI, Fv-antibodies were detected by FITC, and β-TC-6 cells were visualized by mCherry; merged images are shown. (b) Intracellular cAMP accumulation, (c) insulin secretion, and (d) glucagon secretion from α/β co-spheroids under low (2.8 mM) and high (16.7 mM) glucose conditions after treatment with Fv-5, Fv-8, Ex-4, semaglutide, or tirzepatide (1 μM each).

The agonist activity of GLP-1 mimotopes in co-spheroids was assessed by measuring intracellular cAMP levels and hormone secretion under low (2.8 mM) and high (16.7 mM) glucose conditions after treatment with Fv-5, Fv-8, Ex-4, semaglutide, and tirzepatide (1 μM each). As shown in Fig. 5(b), intracellular cAMP accumulation increased upon treatment with all GLP-1R agonists and expressed Fv-antibodies under both glucose conditions.

Under low glucose (2.8 mM) conditions, the cAMP level in the glucose-matched control (NC) was 24.2 nM, and cAMP increased by approximately 1.9-fold with Fv-5 and Fv-8, 2.2-fold with Ex-4, and 2.1-fold with semaglutide and tirzepatide. Under the high glucose (16.7 mM) condition, the control (NC) cAMP level was 36.6 nM, and cAMP increased by approximately 1.5-fold with Fv-5, 1.4-fold with Fv-8, 1.7-fold with Ex-4, 1.6-fold with semaglutide, and 1.4-fold with tirzepatide. As shown in Fig. 5(c), insulin secretion was enhanced in the α/β co-spheroids following treatment with GLP-1R agonists and expressed Fv-antibodies.

Under the low glucose (2.8 mM) condition, the insulin level in the glucose-matched control (NC) was 5.2 ng mL^{-1}, and insulin secretion increased by approximately 2.8-fold with Fv-5, 3.3-fold with Fv-8, 3.5-fold with Ex-4, 3.7-fold with semaglutide, and 3.2-fold with tirzepatide. Under the high glucose (16.7 mM) condition, the control insulin level was 7.9 ng mL^{-1}, and insulin secretion increased by approximately 2.2-fold with Fv-5, 2.4-fold with Fv-8, 2.7-fold with Ex-4 and semaglutide, and 2.5-fold with tirzepatide. As shown in Fig. 5(d), glucagon secretion was suppressed under both glucose conditions. Under the low glucose (2.8 mM) condition, the glucagon level in the glucose-matched control (NC) was 33.7 pg mL^{-1}, and glucagon secretion decreased by approximately 15.0% with Fv-5, 20.2% with Fv-8, 38.3% with Ex-4, 33.5% with semaglutide, and 27.0% with tirzepatide.

Under the high glucose (16.7 mM) condition, the control glucagon level was 22.5 pg mL^{-1}, and glucagon secretion decreased by approximately 35.6% with Fv-5, 39.1% with Fv-8,

52.9% with Ex-4, 50.2% with semaglutide, and 44.9% with tirzepatide. These results confirmed that Fv-5 and Fv-8 induced agonist-like signaling and endocrine outputs in the 3D α/β co-spheroid model, including cAMP and insulin secretion with concomitant glucagon suppression.

3.4. Western blot analysis of GLP-1R downstream signaling (AKT and ERK1/2)

GLP-1R activation has been reported to modulate intracellular kinase signaling in β-cells, including the PI3K-AKT and ERK1/2 pathways. Phosphorylation of AKT (Ser473) and ERK1/2 (Thr202/Tyr204) is commonly used as an early readout of receptor engagement and downstream signaling activity.[68,69] Upon ligand binding, GLP-1R couples to heterotrimeric G proteins, and activation of Gαs stimulates adenylate cyclase (AC) to increase intracellular cAMP, which subsequently activates PKA and Epac. These cAMP-dependent effectors can promote ERK1/2 phosphorylation through downstream signaling intermediates. In parallel, GLP-1R stimulation can engage PI3K signaling, including routes mediated by released Gβγ subunits, leading to AKT phosphorylation[70,71] (Fig. 6(a)).

As shown in Fig. 6(b), treatment with Fv-5, Fv-8, or Ex-4 (1 μM) for 1 h increased the phosphorylation levels of AKT (Ser473) and ERK1/2 (Thr202/Tyr204) in beta-TC-6 cells under both glucose conditions, while the total AKT and ERK levels remained comparable across conditions with β-actin as a loading control. The phosphorylation signals were quantified as p-AKT/AKT/β-actin and p-ERK/ERK/β-actin, and each glucose-matched control was normalized to 1.00. Under the high glucose (16.7 mM) condition, p-AKT increased to 1.30-fold for Fv-5, 1.96-fold for Fv-8, and 1.34-fold for Ex-4 relative to the normalized control, and p-ERK increased to 2.37-fold for Fv-5, 1.56-fold for Fv-8, and 1.37-fold for Ex-4. Under the low glucose (2.8 mM) condition, p-AKT changed to 0.95-fold for Fv-5, 1.14-fold for Fv-8, and 1.23-fold for Ex-4 compared with the normalized control, whereas p-ERK increased to 2.32-fold for Fv-5 and 1.65-fold for Fv-8 but decreased to 0.78-fold for Ex-4. These results indicated that the expressed Fv-antibodies modulated GLP-1R-associated intracellular signaling readouts, with robust ERK phosphorylation and glucose-dependent changes in AKT phosphorylation.

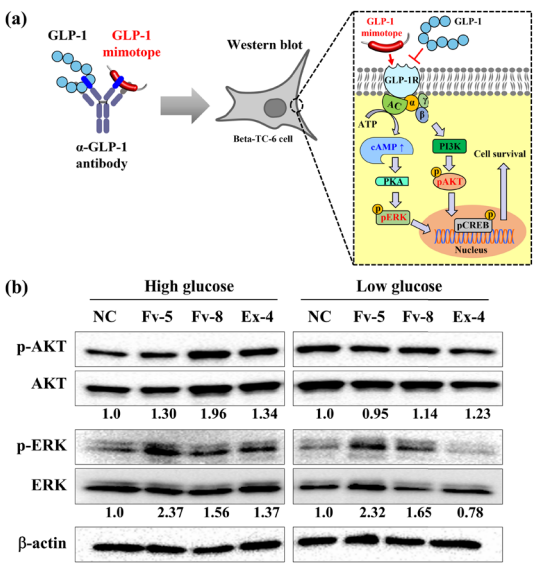

Fig. 6 Western blot analysis of GLP-1R downstream signaling (AKT and ERK1/2) in beta-TC-6 cells under low and high glucose conditions. (a) Schematic of GLP-1R activation by GLP-1 mimotopes and representative downstream signaling routes leading to ERK1/2 and AKT phosphorylation. (b) Western blot of p-AKT (Ser473), total AKT, p-ERK1/2 (Thr202/Tyr204), total ERK1/2, and β-actin in beta-TC-6 cells treated with Fv-5, Fv-8, or Ex-4 (1 μM, 1 h) under high glucose (16.7 mM, left) and low glucose (2.8 mM, right) conditions, with relative band intensity values shown below each blot (each glucose-matched NC set to 1.00).

3.5. Molecular docking simulation of GLP-1 mimotopes and GLP-1R

The interactions between GLP-1R and GLP-1 mimotopes were analyzed by Autodock Vina (Scripps Research Institute, La Jolla, CA, USA).[72–74] All docking results were visualized using PyMOL (version 3.0, Schrödinger, LLC) and further analyzed through Discovery Studio Visualizer (v21.1.0.20298, Dassault Systèmes BIOVIA, San Diego, CA, USA) to identify key interactions. The 11-residue CDR3 sequences of the expressed Fv-antibodies were selected as docking ligands, based on their pivotal role in antigen recognition.

The crystal structure of the active state of GLP-1R (PDB ID: 5VAI) was used for docking, as ligand binding induces a conformational change from the inactive to the active state, thereby initiating receptor activation. GLP-1R is composed of an extracellular domain (ECD) and a transmembrane domain (TMD), which cooperate in ligand binding and signal transduction.[75] The ECD facilitates ligand recognition and capture, while the TMD is responsible for downstream signaling. Previous studies have identified key residues involved in GLP-1 binding, including L_{32}, W_{39}, D_{67}, R_{121}, L_{123}, E_{127}, E_{128}, L_{201}, W_{297}, R_{299}, N_{300}, and R_{380}.[76,77]

As shown in Fig. 7(a), GLP-1 formed multiple interactions with GLP-1R, including nine hydrogen bonds (L_{32}, Y_{88}, R_{121}, E_{138}, K_{197}, W_{297}, T_{298}, R_{299}, and W_{306}), twelve hydrophobic interactions (W_{39}, L_{89}, L_{118}, L_{123}, C_{126}, L_{142}, L_{201}, M_{204}, Y_{241}, I_{309}, R_{310}, and I_{313}), and two electrostatic interactions (E_{128} and E_{139}). The binding affinity of GLP-1 to GLP-1R was calculated to be -13.5 kcal mol^{-1}. Notably, eight of these interacting residues (L_{32}, W_{39}, R_{121}, L_{123}, E_{128}, L_{201}, W_{297}, and R_{299}) matched previously reported key binding sites for GLP-1. As shown in Fig. 7(b), GLP-1 mimotope Fv-5 (only CDR3 region) also formed specific interactions with GLP-1R, including seven hydrogen bonds (L_{142}, Q_{234}, W_{297}, T_{298}, R_{299}, N_{300}, and F_{367}), four hydrophobic interactions (V_{237}, W_{306}, R_{310}, and L_{314}), and three electrostatic interactions (K_{197}, E_{364}, and E_{387}).

The binding affinity of Fv-5 was calculated to be -8.0 kcal mol^{-1}. Among these interacting residues, seven (L_{142}, W_{297}, T_{298}, R_{299}, W_{306}, R_{310}, and K_{197}) overlapped with those involved in GLP-1 binding, suggesting that Fv-5 engaged GLP-1R similarly to GLP-1. As shown in Fig. 7(c), GLP-1 mimotope Fv-8 (only CDR3 region) formed four hydrogen bonds (T_{29}, L_{197}, C_{296}, and W_{297}),

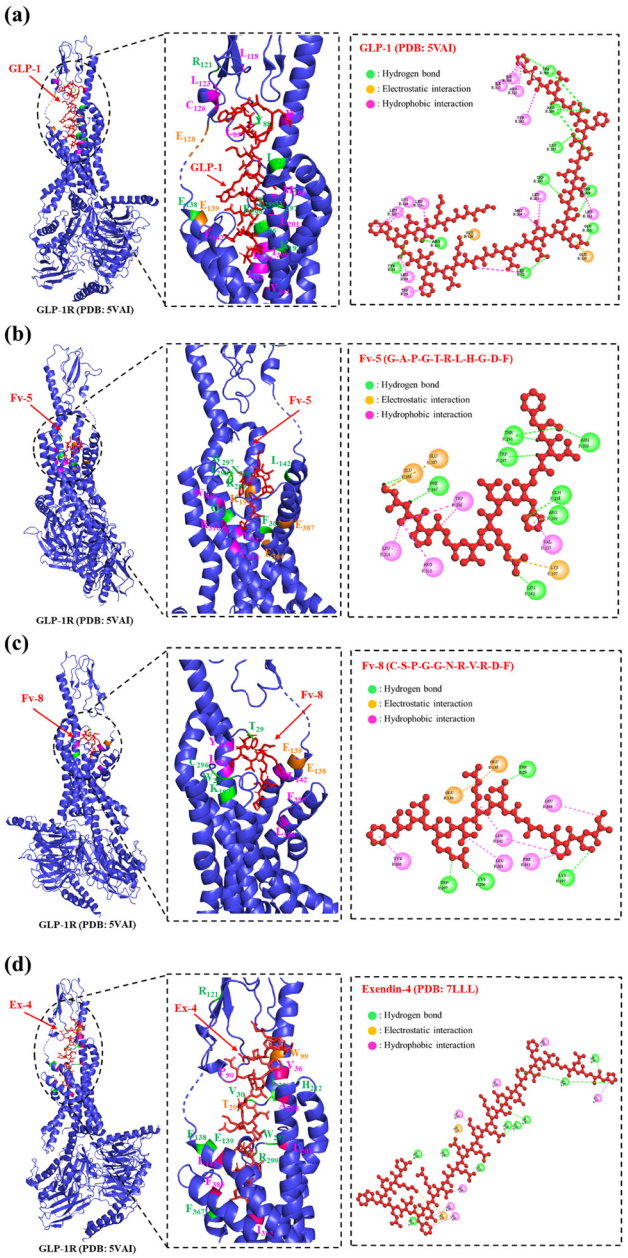

Fig. 7 Molecular docking simulation of GLP-1 or screened GLP-1 mimotopes and GLP-1R (PDB ID: 5VAI). Molecular docking interactions between GLP-1R and (a) GLP-1, (b) GLP-1 mimotope Fv-5, (c) GLP-1 mimotope Fv-8, and (d) Exendin-4.

five hydrophobic interactions (L_{142}, L_{201}, Y_{205}, F_{385}, and L_{388}), and two electrostatic interactions (E_{138} and E_{139}) with GLP-1R. The binding affinity of Fv-8 was calculated to be -8.1 kcal mol^{-1}. Notably, five interacting residues (L_{142}, L_{197}, C_{296}, W_{297}, and L_{201}) overlapped with those involved in GLP-1 binding, indicating that Fv-8 also targeted the functionally relevant regions of the GLP-1 receptor.

The Exendin-4 (PDB ID: 7LLL) was additionally docked to the active-state GLP-1R structure (PDB ID: 5VAI) under the same conditions. Previous structural studies have reported that Ex-4 engages GLP-1R through residues in both the ECD (L_{32}, W_{39}, D_{67}, R_{121}, L_{123}, E_{127}, E_{128}) and the TMD/ECL region (Y_{145}, R_{190}, Q_{211}, H_{212}, W_{297}, R_{299}, L_{388}, S_{392}).[78,79] As shown in Fig. 7(d), Ex-4 formed nine hydrogen-bond interactions with GLP-1R residues (V_{30}, L_{32}, R_{121}, E_{138}, E_{139}, H_{212}, W_{297}, R_{299}, and F_{367}), seven hydrophobic interactions (V_{36}, P_{90}, L_{142}, L_{201}, A_{208}, I_{313}, and F_{385}), and two electrostatic interactions (T_{29} and W_{39}). The binding affinity of Ex-4 was calculated to be -10.1 kcal mol^{-1}. Notably, several interacting residues overlapped with previously reported binding sites, including the ECD residues L_{32}, W_{39}, and R_{121}, as well as the TMD pocket residues W_{297} and R_{299}. These results supported that the docking analysis reproduced the expected binding topology of a validated GLP-1R agonist and provided a reference interaction map for comparison with the screened mimotopes. These docking interactions are summarized in Table 4.

3.6. Effect of GLP-1 mimotopes on the cellular fatty acid accumulation

The effect of GLP-1 mimotopes on lipid accumulation in liver cells was estimated. Excessive accumulation of fat in the liver causes hepatic steatosis or fatty liver, which is attributed to an imbalance between the uptake and removal of fatty acids.[80,81] GLP-1 has been reported to prevent fatty acid accumulation in liver cells through the activation of AMP-activated protein kinase, inhibition of SREBP-1c-mediated lipogenesis, and enhancement of fatty acid oxidation *via* the upregulation of carnitine palmitoyltransferase 1.[82–84]

In this study, the influence of GLP-1 mimotopes on lipid accumulation was estimated using two liver cell lines, namely, HepG2 and Huh7. The liver cells were cultured under 300 μM oleic acid (OA) for 24 h, and the accumulated cellular fatty acid vesicles were stained with Oil red O (Fig. 8(a)). The quantitative amount of accumulated fatty acids in the stained cell lysate was estimated by measuring the absorbance at 510 nm. The influence of GLP-1 mimotopes on fatty acid accumulation was evaluated by treating GLP-1 mimotopes with OA. For HepG2, the level of fatty acids decreased to 28.7 and 28.3% for Fv-5 and Fv-8, respectively, compared to the level of fatty acids without mimotope treatment. When Ex-4 was used as a positive control, the level of fatty acids decreased to 27.8%, as shown in Fig. 8(b). The same experiment was conducted using Huh7, wherein the level of fatty acids decreased to 28.3 and 33.3% for Fv-5 and Fv-8, respectively, compared to the level of fatty acids without mimotope treatment. When Ex-4 was used, the fatty acid levels decreased to 26.0%, as shown in Fig. 8(c). These results showed that GLP-1 mimotopes in the structure of the Fv-antibody effectively prevented the accumulation of cellular fatty acids, similar to that with Ex-4.

The effect of GLP-1 mimotopes on protein expression post-treatment was analyzed *via* mRNA expression analysis. Differentially expressed genes were identified in HepG2 cells treated with Fv-5, Fv-8, or Ex-4 in combination with OA relative to OA-treated HepG2 cells. From a total of 19 925 genes, those exhibiting a fold change >1.5 and a p-value <0.05 were considered significantly dysregulated. Compared to untreated HepG2 cells, OA treatment led to significant dysregulation of

Table 4 Interactions of GLP-1R with GLP-1, GLP-1 mimotopes (Fv-5 and Fv-8), and Ex-4 identified by molecular docking analyses

Agonist	Hydrogen bond	Hydrophobic interaction	Electrostatic interaction	Binding affinity (kcal mol^{-1})
GLP-1	L_{32}, Y_{88}, R_{121}, E_{138}, K_{197}, W_{297}, T_{298}, R_{299}, W_{306}	W_{39}, L_{89}, L_{118}, L_{123}, C_{126}, L_{142}, L_{201}, M_{204}, Y_{241}, I_{309}, R_{310}, I_{313}	E_{128}, E_{139}	−13.5
Fv-5 (CDR3)	L_{142}, Q_{234}, W_{297}, T_{298}, R_{299}, N_{300}, F_{367}	V_{237}, W_{306}, R_{310}, L_{314}	K_{197}, E_{364}, E_{387}	−8.0
Fv-8 (CDR3)	T_{29}, K_{197}, C_{296}, W_{297}	L_{142}, L_{201}, Y_{205}, F_{385}, L_{388}	E_{138}, E_{139}	−8.1
Ex-4	V_{30}, L_{32}, R_{121}, E_{138}, E_{139}, H_{212}, W_{297}, R_{299}, F_{367}	V_{36}, P_{90}, L_{142}, L_{201}, A_{208}, I_{313}, F_{385}	T_{29}, W_{39}	−10.1

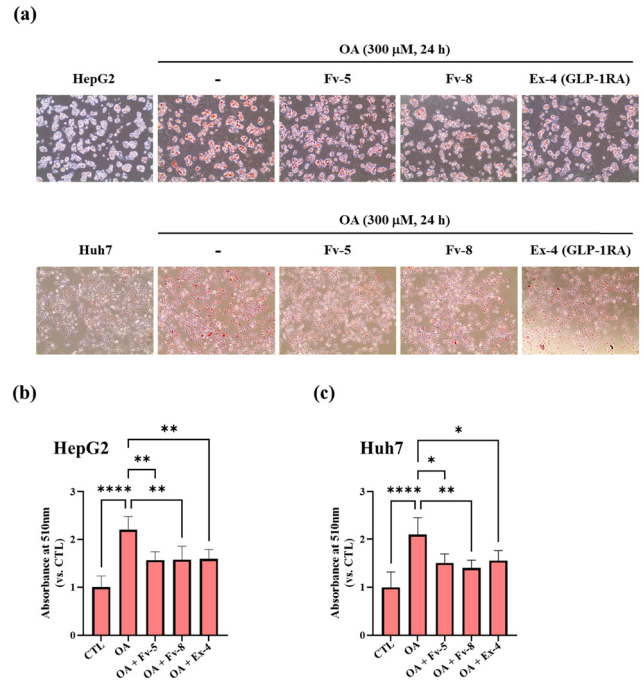

Fig. 8 Inhibitory effect of GLP-1 mimotopes on oleic acid-induced lipid accumulation in liver cell lines (HepG2, Huh7). (a) Oil Red O staining of HepG2 cells and Huh7 cells treated with GLP-1 mimotopes (Fv-5, Fv-8) or Ex-4 under 300 μM oleic acid for 24 h. Quantification of intracellular fatty acid accumulation in (b) HepG2 and (c) Huh7 cells under the same conditions.

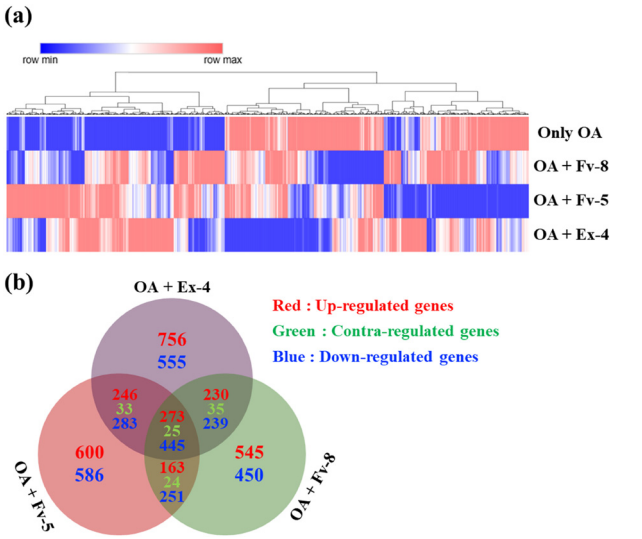

Fig. 9 Transcriptomic analysis of HepG2 cells co-treated with GLP-1 mimotopes (Fv-5, Fv-8) or Ex-4 and oleic acid. (a) Heatmap of differentially expressed genes (DEGs; FC > 1.5, $p < 0.05$) in HepG2 cells treated with Fv-5, Fv-8, or Ex-4 in the presence of oleic acid (OA), compared to OA-only treatment. (b) Venn diagrams showing the distribution of upregulated (red), downregulated (blue), and contra-regulated (green) genes across Fv-5, Fv-8, and Ex-4 co-treatment conditions.

1953 genes. Additionally, co-treatment with OA and Fv-5, Fv-8, or Ex-4 in HepG2 cells significantly altered the expression of 2929, 2680, and 3120 genes, respectively, compared to that of OA-treated HepG2 cells. Co-treatment of Fv-5 with OA exhibited a transcriptional dysregulation pattern more similar to that of Ex-4 than that of co-treated Fv-8 with OA (Fig. 9(a)). Transcriptomic analysis revealed that 519 genes were upregulated and 728 genes downregulated in HepG2 cells co-treated with OA and either Fv-5 or Ex-4. Only 58 genes showed divergent expression patterns between the two co-treatment conditions. Similarly, in HepG2 cells co-treated with OA and either Fv-8 or Ex-4, 503 genes were upregulated, 684 genes were downregulated, and 60 genes exhibited divergent expression patterns (Fig. 9(b)).

Apoptosis in hepatocytes represents a hallmark of fatty liver disease.[85] In HepG2 cells, a widely used hepatic model, exposure to OA induces steatosis and concomitantly enhances apoptotic cell death.[86] Transcriptomic profiling identified 277 genes that were significantly dysregulated in HepG2 cells treated with Fv-5, Fv-8, or Ex-4 with OA compared to those of the OA-treated controls (Fig. 10(a)). Among these, *bcl11b*, which was markedly suppressed upon OA exposure (FC: 0.46 *vs.* CTL), exhibited increased levels following treatment with Fv-5 (FC: 2.03 *vs.* CTL), Fv-8 (FC: 1.76 *vs.* CTL), and Ex-4 (FC: 1.69 *vs.* CTL). The downregulation of *bcl11b* has been implicated as a driver of apoptosis.[87] Additionally, canonical proapoptotic genes, including FAS, TNFRSF25, and CASP9, which were transcriptionally upregulated in response to OA-induced lipotoxic stress, were substantially attenuated by treatment with Fv-5, Fv-8, or Ex-4.[85,88,89]

In hepatocytes affected by non-alcoholic fatty liver disease (NAFLD), lipid accumulation is known to correlate with elevated levels of reactive oxygen species (ROS).[90] Comparative transcriptomic analysis revealed that 60 genes were significantly dysregulated in Fv-5, Fv-8, and Ex-4 treated with OA in HepG2 cells relative to OA-treated controls (Fig. 10(b)).

Among these, key antioxidant genes such as *GPX1*, *FOXO3*, and *SIRT2*, which were typically downregulated following OA treatment, were notably upregulated upon treatment with Fv-antibodies.[91–93]

Ferroptosis, an iron-dependent, non-apoptotic form of regulated cell death, has been increasingly recognized for its

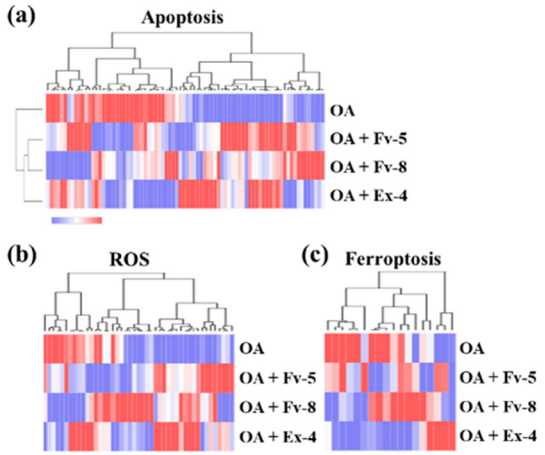

Fig. 10 Transcriptomic analysis of apoptosis, oxidative stress, and ferroptosis pathways in HepG2 cells co-treated with GLP-1 mimotopes (Fv-5, Fv-8) or Ex-4 and oleic acid. Differential expression of genes related to (a) apoptosis, (b) oxidative stress, and (c) ferroptosis.

association with ROS generation.[94] Emerging evidence has implicated ferroptosis in the progression of NAFLD.[95] In this context, 65 genes were significantly dysregulated in Fv-treated with OA *versus* OA-treated HepG2 cells (Fig. 10(c)).

Recent studies identified the transcription factor BACH1 as a critical regulator of ferroptosis under oxidative stress.[96] *BACH1* expression was elevated following OA treatment; however, it was significantly suppressed in cells treated with Fv-5, Fv-8, or Ex-4, suggesting a potential mechanism by which these compounds modulated ferroptotic pathways in NAFLD. Database for Annotation, Visualization, and Integrated Discovery (DAVID) functional annotation analysis was conducted to evaluate the impact of the Fv-antibodies. Analysis comparing Fv-5 and OA co-treated HepG2 cells with OA-treated controls identified significant dysregulation of genes associated with key biological processes (Gene ontology (GO) terms of BP). Impaired calcium signaling has recently been recognized as a key driver of enhanced endoplasmic reticulum (ER) stress, contributing to hepatic lipid accumulation. This dysfunction is closely linked to mitochondrial impairment and autophagic defects, highlighting its potential role in NAFLD.[97,98]

Co-treatment with Fv-5 and OA in HepG2 cells results in significant dysregulation of genes associated with ER calcium ion concentration, lipid metabolic processes, and autophagy compared with OA-treated controls (Fig. 11(a)). Co-treatment with Fv-8 and OA leads to marked alterations in gene expression linked to autophagy, lipid metabolism, and ROS pathways (Fig. 11(b)). Co-treatment with Ex-4 and OA resulted in the dysregulation of pathways commonly observed with Fv-5 and Fv-8 (Fig. 11(c)). Comparative transcriptomic analysis identified 743 genes that were consistently dysregulated in HepG2 cells treated with Ex-4, Fv-5, or Fv-8 compared to those in OA-treated controls.

Among these, 273 genes were upregulated, 445 genes were downregulated, and 25 genes exhibited opposite expression. GO analysis of these genes showed significant enrichment in lipid-associated pathways, including the apoptotic pathway, pathways related to autophagy, and the MAPK signaling pathway (Fig. 11(d)). Consistently, KEGG pathway analysis further confirmed the involvement of these genes in the MAPK signaling pathway, which regulates various aspects of hepatic metabolism. MAPK activation in response to cellular stress impairs the action of insulin and disrupts lipid metabolism. In mouse models with MAPK pathway abnormalities, increased hepatic triglyceride accumulation led to the development of hepatic steatosis (Fig. 11(d)).[99,100]

Additionally, genes associated with the Rap1 signaling pathway were dysregulated. This pathway plays a critical role in the

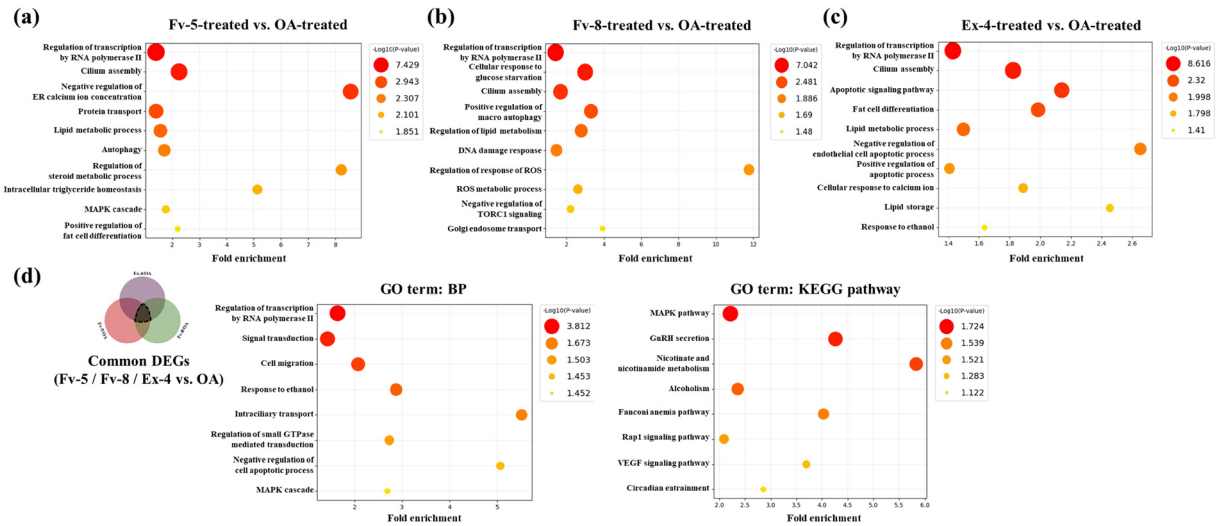

Fig. 11 Gene ontology (GO) and KEGG pathway analysis of dysregulated genes in HepG2 cells co-treated with GLP-1 mimotopes (Fv-5, Fv-8) or Ex-4 and oleic acid. GO biological process (BP) analysis of genes dysregulated by co-treatment of OA with (a) Fv-5, (b) Fv-8, and (c) Ex-4. (d) GO enrichment analysis of commonly dysregulated genes among Fv-5, Fv-8, and Ex-4 treatments (left), and KEGG pathway enrichment analysis of the same gene set (right).

regulation of hepatocyte and adipose tissue functions, and its impairment is linked to liver steatosis, glucose intolerance, insulin resistance, and excessive fat accumulation.[101] The GO term analysis of the disease category identified genes associated with intrahepatic cholestasis ($P < 0.05$), suggesting its potential implications.

4. Conclusions

In this study, GLP-1 mimotopes were screened from an Fv-antibody library using a monoclonal anti-GLP-1 antibody. The screened amino acid sequences (CDR3 sequences, 11 residues) were synthesized into peptides and expressed as Fv-antibodies co-expressed with GFP. The K_D values of GLP-1 mimotopes were analyzed using an SPR biosensor, and K_D was determined to be 71.3 nM for Fv-5 and 62.8 nM for Fv-8, which was similar to that of Ex-4 (66.1 nM). The K_D of synthetic peptides was estimated to be higher than that of Fv-antibodies. These results confirmed that the two Fv-antibodies had a comparable K_D in comparison to that of Ex-4. The inhibitory activity of the GLP-1 mimotopes (synthesized peptides and expressed Fv-antibodies) was analyzed by measuring cAMP production and insulin secretion in beta-TC-6 cells. The EC_{50} values indicated that GLP-1 mimotopes in the structure of Fv-antibodies had higher agonist activity than synthesized peptides with the same CDR3 amino acid sequences. This difference in agonist activity results from differences in K_D between the Fv-antibodies and synthesized peptides.

In addition, the glucagonostatic activity of the expressed Fv-antibodies was evaluated in alpha-TC-1 clone 6 cells by measuring glucagon secretion under low- and high-glucose conditions. To further assess their activity in a more physiologically relevant model, α/β co-spheroids composed of alpha-TC-1 clone 6 and beta-TC-6 cells were established, and intracellular cAMP accumulation as well as insulin and glucagon secretion were quantified. Moreover, GLP-1R downstream signaling was examined in beta-TC-6 cells by western blot analysis of AKT and ERK1/2 phosphorylation.

The molecular docking analyses supported the agonist function of GLP-1 mimotopes by demonstrating their effective binding to the active conformation of GLP-1R. Both Fv-5 and Fv-8 engaged key residues involved in GLP-1 binding with binding affinities of −8.0 and −8.1 kcal mol^{-1}, respectively. These findings suggested that GLP-1 mimotopes mimicked the binding characteristics of GLP-1 and contributed to receptor activation through similar molecular interactions.

The effect on fatty acid accumulation was analyzed using liver cell lines, such as HepG2 and Huh7. Both cell lines showed that the level of fatty acids decreased to 28–33% in comparison with the level of fatty acids without mimotope treatment (Ex-4 reduced 26.0%).

These results confirmed that GLP-1 mimotopes in the structure of the Fv-antibody could effectively prevent the accumulation of cellular fatty acids as high as Ex-4. The effect of GLP-1 mimotopes on protein expression was analyzed by the mRNA expression analysis of OA-treated HepG2 cells. Comparative transcriptomic analysis revealed that 743 genes were significantly dysregulated in Fv-5, Fv-8, and Ex-4 treated with OA in HepG2 cells in comparison with only OA-treated controls. Several genes have been reported to play critical roles in regulating hepatocyte and adipose tissue functions linked to liver steatosis, glucose intolerance, insulin resistance, and excessive fat accumulation.

Conflicts of interest

The authors declare no conflicts of interest.

Data availability

All data generated or analyzed during this study are included in this published article and its supplementary information (SI) files. Supplementary information is available. See DOI: https://doi.org/10.1039/d5tb02128f.

Acknowledgements

This work was supported by the National Research Foundation of Korea [grant numbers RS-2023-00209053, NRF-2020R1A5A1019 13111, and NRF2022K1A3A1A25081295]; and the Korea Health Industry Development Institute (KHIDI) of Korea [grant numbers HI19C1344, and RS-2025-02213534]. This study was jointly supported by the Gangnam Severance Hospital and the Institute of Engineering Research, Yonsei University.

References

1 Z. Zheng, Y. Zong, Y. Ma, Y. Tian, Y. Pang, C. Zhang and J. Gao, *Signal Transduction Targeted Ther.*, 2024, **9**, 234.
2 G. E. Lim and P. L. Brubaker, *Diabetes*, 2006, **55**, S70–S77.
3 T. D. Müller, B. Finan, S. Bloom, D. D'Alessio, D. J. Drucker, P. Flatt, A. Fritsche, F. Gribble, H. Grill and J. Habener, *Mol. Metab.*, 2019, **30**, 72–130.
4 A. Meloni, M. DeYoung, C. Lowe and D. Parkes, *Diabetes, Obes. Metab.*, 2013, **15**, 15–27.
5 R. Ramracheya, C. Chapman, M. Chibalina, H. Dou, C. Miranda, A. González, Y. Moritoh, M. Shigeto, Q. Zhang and M. Braun, *Phys. Rep.*, 2018, **6**, e13852.
6 C. De Graaf, D. Donnelly, D. Wootten, J. Lau, P. M. Sexton, L. J. Miller, J.-M. Ahn, J. Liao, M. M. Fletcher and D. Yang, *Pharmacol. Rev.*, 2016, **68**, 954–1013.
7 P. Nadkarni, O. G. Chepurny and G. G. Holz, *Prog. Mol. Biol. Transl. Sci*, 2014, **121**, 23–65.
8 V. R. Aroda, *Diabetes, Obes. Metab.*, 2018, **20**(Suppl. 1), 22–33.
9 J. Xiang, L. Qin, J. Zhong, N. Xia and Y. Liang, *Diabetes, Metab. Syndr. Obes.: Targets Ther.*, 2023, 2433–2446.
10 L. Ferhatbegović, D. Mršić and A. Macić-Džanković, *Front. Clin. Diabetes Healthc.*, 2023, **4**, 1293926.

11 S. H. Alharbi, *Ther. Adv. Endocrinol. Metab.*, 2024, **15**, 20420188231222367.
12 X. y Liu, L. M. Pop and E. S. Vitetta, *Immunol. Rev.*, 2008, **222**, 9–27.
13 K. Masuda, K. Sakamoto, M. Kojima, T. Aburatani, T. Ueda and H. Ueda, *FEBS J.*, 2006, **273**, 2184–2194.
14 T. W. Mak, M. E. Saunders and B. D. Jett, *Primer to the immune response*, Newnes, 2013.
15 M. L. Fernández-Quintero, J. R. Loeffler, J. Kraml, U. Kahler, A. S. Kamenik and K. R. Liedl, *Front. Immunol.*, 2019, **9**, 3065.
16 H. I. Park, H. W. Yoon and S. T. Jung, *Trends Biotechnol.*, 2016, **34**, 895–908.
17 K. Zhang, X. Yin, K. Shi, S. Zhang, J. Wang, S. Zhao, H. Deng, C. Zhang, Z. Wu and Y. Li, *Sci. Rep.*, 2021, **11**, 10454.
18 Y. Li, M. R. Owen, W. Cockburn, I. Kumagai and G. C. Whitelam, *Protein Eng., Des. Sel.*, 1996, **9**, 1211–1217.
19 J. Jose, *Appl. Microbiol. Biotechnol.*, 2006, **69**, 607–614.
20 M. Gustavsson, E. Bäcklund and G. Larsson, *Microb. Cell Fact.*, 2011, **10**, 1–10.
21 J. Jose and T. F. Meyer, *Microbiol. Mol. Biol. Rev.*, 2007, **71**, 600–619.
22 E. van Bloois, R. T. Winter, H. Kolmar and M. W. Fraaije, *Trends Biotechnol.*, 2011, **29**, 79–86.
23 B. Bakhshinejad, H. M. Zade, H. S. Z. Shekarabi and S. Neman, *Amino Acids*, 2016, **48**, 2699–2716.
24 A. B. Riemer and E. Jensen-Jarolim, *Immunol. Lett.*, 2007, **113**, 1–5.
25 M. P. Rudolf, M. Vogel, F. Kricek, C. Ruf, A. W. Zurcher, R. Reuschel, M. Auer, S. Miescher and B. M. Stadler, *J. Immunol.*, 1998, **160**, 3315–3321.
26 H. E. Bae, J. Jung, J. S. Sung, S. Kwon, M.-J. Kang, J. Jose, M. Lee and J.-C. Pyun, *Int. J. Biol. Macromol.*, 2025, 140770.
27 H. E. Bae, J. Jung, J. S. Sung, S. Kwon, M.-J. Kang, J. Jose and J.-C. Pyun, *J. Mater. Chem. B*, 2025, **13**, 6154–6163.
28 S. Rumiński, I. Kalaszczyńska and M. Lewandowska-Szumieł, *Cells*, 2020, **9**, 1587.
29 B. Niu, L. Liu, H. Su, X. Xia, Q. He, Y. Feng, Y. Xue and X. Yan, *Mol. Med. Rep.*, 2016, **13**, 4451–4454.
30 N. Lawlor, A. Youn, R. Kursawe, D. Ucar and M. L. Stitzel, *Sci. Rep.*, 2017, **7**, 11959.
31 R. Guo, Y. Zhang, Y. Yu, S. Su, Q. Zhao, X. Chu, S. Li, H. Lu and C. Sun, *Genes Nutr.*, 2021, **16**, 8.
32 L. S. Ramos, J. H. Zippin, M. Kamenetsky, J. Buck and L. R. Levin, *J. Gen. Physiol.*, 2008, **132**, 329–338.
33 E. P. Pratt, K. E. Harvey, A. E. Salyer and G. H. Hockerman, *PLoS One*, 2019, **14**, e0215188.
34 V. r Serre, W. Dolci, E. Schaerer, L. Scrocchi, D. Drucker, S. Efrat and B. Thorens, *Endocrinology*, 1998, **139**, 4448–4454.
35 S. M. Kim, E. J. Lee, H. S. Jung, N. Han, Y. J. Kim, T. K. Kim, T. N. Kim, M. J. Kwon, S. H. Lee and J. H. Park, *Endocrinol. Metab.*, 2015, **30**, 92–97.
36 Y. Ntamo, E. Samodien, J. Burger, N. Muller, C. J. Muller and N. Chellan, *Front. Cell Dev. Biol.*, 2021, **8**, 623889.
37 J. Kim, S. Park, S. Kim, S. Ryu, H. Hwang, S. Cho, Y. Han, J. Kim, Y. Park and E. K. Lee, *Prostate*, 2024, **84**, 814–822.
38 Y. Park, Y. Han, D. Kim, S. Cho, W. Kim, H. Hwang, H. W. Lee, D. H. Han, K. S. Kim and M. Yun, *Cancers*, 2022, **14**, 1205.
39 D. W. Huang, B. T. Sherman and R. A. Lempicki, *Nat. Protoc.*, 2009, **4**, 44–57.
40 E. M. Herold, C. John, B. Weber, S. Kremser, J. Eras, C. Berner, S. Deubler, M. Zacharias and J. Buchner, *Sci. Rep.*, 2017, **7**, 12276.
41 Z. A. Ahmad, S. K. Yeap, A. M. Ali, W. Y. Ho, N. B. M. Alitheen and M. Hamid, *J. Immunol. Res.*, 2012, **2012**, 980250.
42 J. S. Sung, J. Jung, T.-H. Kim, S. Kwon, H. E. Bae, M.-J. Kang, J. Jose, M. Lee and J.-C. Pyun, *Bioconjugate Chem.*, 2024, **35**, 1324–1334.
43 J. S. Sung, S. Kim, J. Jung, T.-H. Kim, S. Kwon, H. E. Bae, M.-J. Kang, J. Jose, M. Lee and J.-C. Pyun, *ACS Pharmacol. Transl. Sci.*, 2023, **7**, 150–160.
44 J. Jung, J. S. Sung, T.-H. Kim, M.-J. Kang, J. Jose, H.-J. Shin and J.-C. Pyun, *Biochip J.*, 2024, **18**, 318–329.
45 J.-H. Bong, S. J. Lee, J. Jung, J. S. Sung, M.-J. Kang, M. Lee, J. Jose and J.-C. Pyun, *Biochip J.*, 2024, **18**, 146–159.
46 Y. Yoon, Y. Kwon, H. Park, S. Lee, C. Park and T. Lee, *Biochip J*, 2024, **18**, 1–21.
47 K. Nakashima, M. Shimoda, S. Hamamoto, F. Tatsumi, H. Hirukawa, K. Tawaramoto, Y. Kanda and K. Kaku, *Mol. Cell. Endocrinol.*, 2012, **349**, 281–288.
48 S. Rajan, L. M. Dickson, E. Mathew, C. M. Orr, J. H. Ellenbroek, L. H. Philipson and B. Wicksteed, *Mol. Metab.*, 2015, **4**, 265–276.
49 M. Komatsu, M. Takei, H. Ishii and Y. Sato, *J. Diabetes Investig.*, 2013, **4**, 511–516.
50 M. Deepa Maheshvare, S. Raha, M. König and D. Pal, *Front. Endocrinol.*, 2023, **14**, 1185656.
51 R. Carlessi, Y. Chen, J. Rowlands, V. F. Cruzat, K. N. Keane, L. Egan, C. Mamotte, R. Stokes, J. E. Gunton and P. I. H. D. Bittencourt, *Sci. Rep.*, 2017, **7**, 2661.
52 P. E. MacDonald, W. El-Kholy, M. J. Riedel, A. M. F. Salapatek, P. E. Light and M. B. Wheeler, *Diabetes*, 2002, **51**, S434–S442.
53 B. Svendsen and J. J. Holst, *Diabetologia*, 2021, **64**, 142–151.
54 A. Ørgaard and J. J. Holst, *Diabetologia*, 2017, **60**, 1731–1739.
55 Y. Zhang, K. R. Parajuli, G. E. Fava, R. Gupta, W. Xu, L. U. Nguyen, A. F. Zakaria, V. A. Fonseca, H. Wang and F. Mauvais-Jarvis, *Diabetes*, 2019, **68**, 34–44.
56 G. G. Holz, C. A. Leech and J. F. Habener, *J. Biol. Chem.*, 1995, **270**, 17749–17757.
57 V. Poitout, L. E. Stout, M. B. Armstrong, T. F. Walseth, R. L. Sorenson and R. P. Robertson, *Diabetes*, 1995, **44**, 306–313.
58 J. Kolic and P. E. MacDonald, *J. Clin. Investig.*, 2015, **125**, 4327–4330.
59 J. Foote and G. Winter, *J. Mol. Biol.*, 1992, **224**, 487–499.
60 M. Arslan, D. Karadag and S. Kalyoncu, *Proteins: Struct., Funct., Bioinf.*, 2020, **88**, 1447–1457.
61 B. Jones, S. R. Bloom, T. Buenaventura, A. Tomas and G. A. Rutter, *Peptides*, 2018, **100**, 75–84.

62 S. Piro, L. G. Mascali, F. Urbano, A. Filippello, R. Malaguarnera, S. Calanna, A. M. Rabuazzo and F. Purrello, *PLoS One*, 2014, **9**, e90093.
63 P. Rorsman, M. Braun and Q. Zhang, *Cell Calcium*, 2012, **51**, 300–308.
64 L. Briant, A. Salehi, E. Vergari, Q. Zhang and P. Rorsman, *Upsala J. Med. Sci.*, 2016, **121**, 113–119.
65 A. Ørgaard and J. J. Holst, *Diabetologia*, 2017, **60**, 1731–1739.
66 D. J. Drucker, *Cell Metab.*, 2018, **27**, 740–756.
67 Y. Z. De Marinis, A. Salehi, C. E. Ward, Q. Zhang, F. Abdulkader, M. Bengtsson, O. Braha, M. Braun, R. Ramracheya and S. Amisten, *Cell Metab.*, 2010, **11**, 543–553.
68 B. Yusta, L. L. Baggio, J. L. Estall, J. A. Koehler, D. P. Holland, H. Li, D. Pipeleers, Z. Ling and D. J. Drucker, *Cell Metab.*, 2006, **4**, 391–406.
69 S. Dalle and A. Abderrahmani, *Cells*, 2024, **13**, 1244.
70 A. Marzook, A. Tomas and B. Jones, *Front. Endocrinol.*, 2021, **12**, 678055.
71 J. Quoyer, C. Longuet, C. Broca, N. Linck, S. Costes, E. Varin, J. Bockaert, G. Bertrand and S. Dalle, *J. Biol. Chem.*, 2010, **285**, 1989–2002.
72 J. Eberhardt, D. Santos-Martins, A. F. Tillack and S. Forli, *J. Chem. Inf. Model.*, 2021, **61**, 3891–3898.
73 D. S. Goodsell, G. M. Morris and A. J. Olson, *J. Mol. Recognit.*, 1996, **9**, 1–5.
74 O. Trott and A. J. Olson, *J. Comput. Chem.*, 2010, **31**, 455–461.
75 F. Wu, L. Yang, K. Hang, M. Laursen, L. Wu, G. W. Han, Q. Ren, N. K. Roed, G. Lin and M. A. Hanson, *Nat. Commun.*, 2020, **11**, 1272.
76 C. R. Underwood, P. Garibay, L. B. Knudsen, S. Hastrup, G. H. Peters, R. Rudolph and S. Reedtz-Runge, *J. Biol. Chem.*, 2010, **285**, 723–730.
77 D. Wootten, C. A. Reynolds, K. J. Smith, J. C. Mobarec, C. Koole, E. E. Savage, K. Pabreja, J. Simms, R. Sridhar and S. G. Furness, *Cell*, 2016, **165**, 1632–1643.
78 S. Runge, H. Thøgersen, K. Madsen, J. Lau and R. Rudolph, *J. Biol. Chem.*, 2008, **283**, 11340–11347.
79 Y. Zhang, B. Sun, D. Feng, H. Hu, M. Chu, Q. Qu, J. T. Tarrasch, S. Li, T. Sun Kobilka and B. K. Kobilka, *Nature*, 2017, **546**, 248–253.
80 S. Hoffman and K. Adeli, *Med. Rev.*, 2024, **4**, 301–311.
81 T. Bu, Z. Sun, Y. Pan, X. Deng and G. Yuan, *Diabetes Metab. J.*, 2024, **48**, 354–372.
82 R. Li, X. Sun, P. Li, W. Li, L. Zhao, L. Zhu and S. Zhu, *Front. Cell Dev. Biol.*, 2021, **9**, 646113.
83 A. S. Akarte, B. Srinivasan and S. Gandhi, *J. Diabetes Complicat.*, 2012, **26**, 266–274.
84 O. Khalifa, N. S. Al-Akl, K. Errafii and A. Arredouani, *Sci. Rep.*, 2022, **12**, 2226.
85 A. E. Feldstein, A. Canbay, P. Angulo, M. Taniai, L. J. Burgart, K. D. Lindor and G. J. Gores, *Gastroenterology*, 2003, **125**, 437–443.
86 W. Cui, S. L. Chen and K.-Q. Hu, *Am. J. Transl. Res.*, 2010, **2**, 95.
87 R. Kominami, *Proc. Jpn. Acad. Ser. B Phys. Biol. Sci.*, 2012, **88**, 72–87.
88 L. Fang, B. Adkins, V. Deyev and E. R. Podack, *J. Exp. Med.*, 2008, **205**, 1037–1048.
89 M. Brentnall, L. Rodriguez-Menocal, R. L. De Guevara, E. Cepero and L. H. Boise, *BMC Cell Biol.*, 2013, **14**, 1–9.
90 M. Martín-Fernández, V. Arroyo, C. Carnicero, R. Sigüenza, R. Busta, N. Mora, B. Antolín, E. Tamayo, P. Aspichueta and I. Carnicero-Frutos, *Antioxidants*, 2022, **11**, 2217.
91 K. Faucher, H. Rabinovitch-Chable, G. Barriere, J. Cook-Moreau and M. Rigaud, *Biochimie*, 2003, **85**, 611–617.
92 E. C. Ferber, B. Peck, O. Delpuech, G. P. Bell, P. East and A. Schulze, *Cell Death Differ.*, 2012, **19**, 968–979.
93 V. Lemos, R. M. De Oliveira, L. Naia, É. Szegö, E. Ramos, S. Pinho, F. Magro, C. Cavadas, A. C. Rego and V. Costa, *Hum. Mol. Genet.*, 2017, **26**, 4105–4117.
94 J. Li, F. Cao, H.-L. Yin, Z.-J. Huang, Z.-T. Lin, N. Mao, B. Sun and G. Wang, *Cell Death Dis.*, 2020, **11**, 88.
95 S. Wang, Z. Liu, J. Geng, L. Li and X. Feng, *Biomed. Pharmacother.*, 2022, **153**, 113374.
96 H. Nishizawa, M. Yamanaka and K. Igarashi, *FEBS J.*, 2023, **290**, 1688–1704.
97 E. S. Ali and N. Petrovsky, *Trends Endocrinol. Metab.*, 2019, **30**, 270–281.
98 J. Wang, W. He, P.-J. Tsai, P.-H. Chen, M. Ye, J. Guo and Z. Su, *Lipids Health Dis.*, 2020, **19**, 1–19.
99 A. Lawan and A. M. Bennett, *Trends Endocrinol. Metab.*, 2017, **28**, 868–878.
100 T. Kujiraoka, Y. Satoh, M. Ayaori, Y. Shiraishi, Y. Arai-Nakaya, D. Hakuno, H. Yada, N. Kuwada, S. Endo and K. Isoda, *J. Am. Heart Assoc.*, 2013, **2**, e000361.
101 F. Yeung, C. M. Ramírez, P. A. Mateos-Gomez, A. Pinzaru, G. Ceccarini, S. Kabir, C. Fernández-Hernando and A. Sfeir, *Cell Rep.*, 2013, **3**, 1847–1856.